




Multiple-weak-value quantum measurement for precision estimation of time delayYongsheng Wang ¹, Wenshuai Zhang ¹, Shizhen Chen,^{2,*} Shuangchun Wen,² and Hailu Luo ^{1,†}¹Laboratory for Spin Photonics, School of Physics and Electronics, Hunan University, Changsha 410082, China²Key Laboratory for Micro-/Nano-Optoelectronic Devices of Ministry of Education, School of Physics and Electronics, Hunan University, Changsha 410082, China

(Received 19 November 2021; revised 7 March 2022; accepted 10 March 2022; published 25 March 2022)

In quantum weak measurement, a weak value is a quantity related to a pointer shift of a measuring device which is usually determined by pre- and postselection states. For conventional weak measurement, a single weak-value model has been well addressed in precision metrology of time delay, but it only holds for a narrowband light source. To further improve the measurement accuracy, a broad-spectrum light source is needed. We find that the single weak-value model no longer holds, due to the occurrence of modified preselection states. Here, a multiple weak-value model is established by introducing the modified preselection states in the estimation of time delay. For broad-spectrum light source with 50-nm spectral width, the multiple weak-value scheme enables us to achieve a high resolution of 1.6×10^{-4} as. Our proposed multiple weak-value amplification may have important applications in various fields involving precise time-delay detection.

DOI: [10.1103/PhysRevA.105.033521](https://doi.org/10.1103/PhysRevA.105.033521)**I. INTRODUCTION**

High precision estimation of time delay is significant for various fields of modern physics. The detection of time delay is usually carried out in various optical systems including birefringence and interferometer with optical-path change [1,2]. Apart from the traditional methods, the weak measurements as an advanced technique showed a great improvement for the estimation accuracy of time delay. Taking time delay as the measuring pointer could extend it to various systems for other parameter estimation, which holds great application potential in precision metrology [3–9]. To further improve the time-delay sensitivity, the scheme with designative weak value can be performed as a powerful complement.

The concept of weak measurements was formulated by Aharonov, Albert, and Vaidman [10]. An observable was weakly measured in a preselected and postselected ensemble. Such a weak measurement protocol will lead to a peculiar result that is known as weak value. The weak value can lie outside the range of eigenvalues for nearly orthogonal preselection and postselection, and may even be complex [11]. On the one hand, the undisturbed properties of the weak measurements can give possible practical applications, such as the unorthodox prediction, direct measurement of the quantum wave function, and the average trajectories of single photons [12–15]. On the other hand, the excellent weak-value amplification effect has been demonstrated as a tool for precision metrology [16–24]. And the weak-value schemes have been proved to have benefits to improving the accuracy by suppressing technical noise [25–27]. In fact, further improvement

of the accuracy in weak measurements is a longer-term issue. There were some attempts beyond the general weak-value formalism for this aim, including optimization of pointer states, higher-order expansions for nearly orthogonal preselection and postselection, and amplification with recycled photons [28–31]. Among that, the spectral weak measurements with imaginary weak value was discussed to show its superiority for the resolution enhancement, compared with the standard scheme [32]. Since that, some important works based on real or imaginary weak value amplification for applied experiments have sequentially appeared [33–38]. However, in some applications of the weak measurements based on the frequency domain, such as magneto-optical Faraday effect detection and chirality detection, the wavelength-dependent properties require reconsideration when applied to broad-spectrum light sources.

In this paper, the multiple weak value (MWV) scheme is proposed to enable the zero-order quarter-wave plate that can only be operated in single wavelength light to be accurately utilized for a broad-spectrum light source. Different from the standard weak measurements with single weak value (SWV), the multiple weak values with both real and imaginary parts are obtained when considering the modified preselection in a spectral-width light source. In the previous analysis of weak measurements, this effect was usually ignored and the small time delay only enlarged by single real or imaginary weak value. To obtain the MWV amplification, the theory of MWV weak measurements is derived compared with the SWV scheme. Moreover, the preselection angle and the spectral width of the light source have been indicated as significant influences on measurement efficiency [39]. To show the deviation of the MWV and SWV schemes for the detection of small time delay, we discuss the wavelength shift in two sensitive regions with different spectral widths.

*szchen@hnu.edu.cn

†hailuluo@hnu.edu.cn

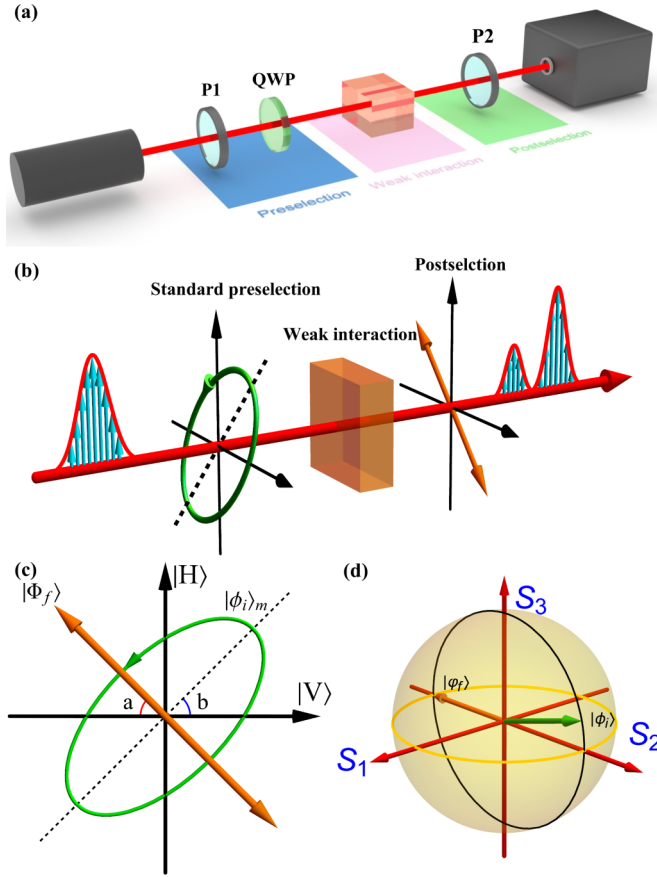


FIG. 1. Diagrams of the experimental setup and theoretical scheme of the SWV. (a) Experimental system illustration of a broad-spectrum weak measurement system based on frequency domain consisting of preselection, weak interaction, and postselection. (b) The conventional single weak-value measurements with standard preselection are presented, where the weak interaction is provided by small time delay τ . (c) Comparison of the standard preselection consisting of elliptical polarization with the postselection of linear polarization, where the magnitudes of angles a and b are $\pi/4$. (d) Presentation of standard preselection and postselection states via the Poincaré sphere.

II. SINGLE WEAK-VALUE MEASUREMENT

In the general weak measurement schemes for time delay estimation, polarization-based measurement systems with spectral distribution are commonly used. As shown in Fig. 1(a), the experimental setup of the frequency-domain weak measurement system based on a broad-spectrum light source consists of three components: the preselection consisting of a line polarizer (P1) and a quarter-wave plate (QWP), the weak interaction caused by the phase difference, and the postselection operated by a linear polarization (P2). The weak value of the observable \hat{A} on the preselected and postselected ensembles $\langle \varphi_f | \phi_i \rangle$ is given by [29,40,41]

$$A_\omega = \frac{\langle \varphi_f | \hat{A} | \phi_i \rangle}{\langle \varphi_f | \phi_i \rangle}, \quad (1)$$

where the mutual coupling of $\langle \varphi_f | \phi_i \rangle$ determines the strength of amplification and the signal-to-noise ratio. Here, we

consider the weak interaction procedure is introduced by a birefringent crystal. A small time delay is induced between the horizontal polarization ($|H\rangle$) and vertical polarization ($|V\rangle$) after the interaction. Thus, the observable operator \hat{A} is $|H\rangle\langle H| - |V\rangle\langle V|$. P1 is set to $\pi/4 + \varepsilon$, and Jones matrix can be written as

$$\begin{aligned} & \begin{bmatrix} \cos(\frac{\pi}{4} + \varepsilon) & -\sin(\frac{\pi}{4} + \varepsilon) \\ \sin(\frac{\pi}{4} + \varepsilon) & \cos(\frac{\pi}{4} + \varepsilon) \end{bmatrix} \begin{bmatrix} 1 & 0 \\ 0 & 0 \end{bmatrix} \\ & \times \begin{bmatrix} \cos(\frac{\pi}{4} + \varepsilon) & \sin(\frac{\pi}{4} + \varepsilon) \\ -\sin(\frac{\pi}{4} + \varepsilon) & \cos(\frac{\pi}{4} + \varepsilon) \end{bmatrix} \\ & = \begin{bmatrix} \cos^2(\frac{\pi}{4} + \varepsilon) & \frac{1}{2} \cos 2\varepsilon \\ \frac{1}{2} \cos 2\varepsilon & \sin^2(\frac{\pi}{4} + \varepsilon) \end{bmatrix}. \end{aligned} \quad (2)$$

For QWP with an angle of $\pi/4$, the retardation for the central wavelength of light source is $\Gamma_0 = \pi/2$, and the corresponding matrix becomes

$$\begin{aligned} & \begin{bmatrix} \cos \frac{\pi}{4} & -\sin \frac{\pi}{4} \\ \sin \frac{\pi}{4} & \cos \frac{\pi}{4} \end{bmatrix} \begin{bmatrix} e^{-i\frac{\Gamma_0}{2}} & 0 \\ 0 & e^{-i\frac{\Gamma_0}{2}} \end{bmatrix} \begin{bmatrix} \cos \frac{\pi}{4} & \sin \frac{\pi}{4} \\ -\sin \frac{\pi}{4} & \cos \frac{\pi}{4} \end{bmatrix} \\ & = \begin{bmatrix} \cos \frac{\pi}{4} & -i \sin \frac{\pi}{4} \\ -i \sin \frac{\pi}{4} & \cos \frac{\pi}{4} \end{bmatrix}. \end{aligned} \quad (3)$$

Thus, the Jones matrix of standard preselection could be obtained as

$$\begin{aligned} |\phi_i\rangle & = \begin{bmatrix} \cos \frac{\pi}{4} & -i \sin \frac{\pi}{4} \\ -i \sin \frac{\pi}{4} & \cos \frac{\pi}{4} \end{bmatrix} \\ & \times \begin{bmatrix} \cos^2(\frac{\pi}{4} + \varepsilon) & \frac{1}{2} \cos 2\varepsilon \\ \frac{1}{2} \cos 2\varepsilon & \sin^2(\frac{\pi}{4} + \varepsilon) \end{bmatrix} \begin{bmatrix} 1 \\ 1 \end{bmatrix} \\ & = \begin{bmatrix} e^{-i\varepsilon} \\ e^{i\varepsilon} \end{bmatrix}. \end{aligned} \quad (4)$$

To realize the standard single weak-value amplification, an appropriate postselection nearly orthogonal to the preselection is selected by a polarizer with angle $-\pi/4$. And we have

$$|\phi_i\rangle = \frac{1}{\sqrt{2}}(e^{-i\varepsilon}|H\rangle + e^{i\varepsilon}|V\rangle), \quad (5)$$

$$|\varphi_f\rangle = \frac{1}{\sqrt{2}}(|H\rangle - |V\rangle). \quad (6)$$

This standard single weak-value measurement scheme with both the standard pre- and postselection is shown in Fig. 1(b). The initial state first passes through the preselection. Then, after the weak interaction with a birefringent crystal, it undergoes a 2τ time-delay difference between the $|H\rangle$ and $|V\rangle$ components. Finally, the postselection performs projection observation and the wave function with two completely separating peaks experiences a frequency shift. Substituting the standard preselection and postselection into Eq. (1), the SWV can be obtained as

$$A_\omega = i \cot \varepsilon. \quad (7)$$

Here, it is assumed that the incident spectral distribution is Gaussian:

$$f(\omega) = \frac{1}{\sqrt{\pi}\sigma^2} \exp\left[-\frac{(\omega - \omega_0)^2}{2\sigma^2}\right], \quad (8)$$

wherein the relationship between ω_0 and central spectrum wavelength λ_0 is $\omega_0 = 2\pi c/\lambda_0$. And the σ corresponds to the width of the wave function. The standard preselection state with the incident spectral distribution is expressed as

$$|\psi\rangle = \frac{1}{\sqrt{2}} \int d\omega f(\omega)[e^{-i\varepsilon}|H\rangle + e^{i\varepsilon}|V\rangle]|\omega\rangle. \quad (9)$$

Then, the time delay of 2τ is introduced by the weak interaction on $|H\rangle$ and $|V\rangle$ and the wave function becomes

$$|\psi'\rangle = \frac{1}{\sqrt{2}} \int d\omega f(\omega)[e^{i(\tau\omega-\varepsilon)}|H\rangle + e^{-i(\tau\omega-\varepsilon)}|V\rangle]|\omega\rangle. \quad (10)$$

After postselection is applied, the probe state collapses to

$$\langle\varphi_f|\psi'\rangle = \frac{1}{2} \int d\omega f(\omega)[e^{i(\tau\omega-\varepsilon)} - e^{-i(\tau\omega-\varepsilon)}]|\omega\rangle. \quad (11)$$

In this case, the postselection probability is obtained as

$$\begin{aligned} T &= \int P_f(\omega)d\omega = |\langle\varphi_f|\psi'\rangle|^2 \\ &= \frac{1}{2}[1 - e^{-\sigma^2\tau^2} \cos(2\varepsilon - 2\tau\omega_0)]. \end{aligned} \quad (12)$$

Therefore, the frequency shift can be calculated as

$$\Delta\omega = \frac{\int \omega P_f(\omega)d\omega}{\int P_f(\omega)d\omega} - \omega_0 = \frac{\tau\sigma^2}{2T} e^{-\tau\sigma^2} \sin(2\tau\omega_0 - 2\varepsilon). \quad (13)$$

As a result, the wavelength shift corresponding to the time delay τ and standard preselection angle ε present is given by

$$\Delta\lambda = -\frac{\lambda_0^2}{2\pi c} \Delta\omega = \frac{e^{-\tau^2\sigma^2} \lambda_0^2 \tau \sigma^2 \sin(2\varepsilon - 2\tau\omega_0)}{2\pi c [1 - e^{-\tau^2\sigma^2} \cos(2\varepsilon - 2\tau\omega_0)]}. \quad (14)$$

From Eq. (14), the variation of wavelength shift caused by the time delay has the periodic change with $(\varepsilon - \pi)/\omega_0$. In this paper, the linear region of wavelength shift around $\tau = (\varepsilon - n\pi)/\omega_0$ ($n = 0, 1, 2, \dots$) is defined as working region since the time-delay change in this region is very sensitive. With the increase of time delay, the trend of wavelength shift in the working region is almost the same, and only the span of period becomes gradually broader.

The frequency-domain weak measurement scheme based on the SWV maintains the ability to measure minimal time delay in the linear amplification region precisely. In the working region with positive integers n , the SWV simulation was consistent with the detection [34,39]. However, the final received waveform spectrum under the situation of $n = 0$ is partial overlap, it may be a discrepancy with the SWV theory. In this case, to confirm the high measurement accuracy, these two working regions with $n = 0$ and 1 are discussed. For brevity, the working region of $n = 0$ is named Zone 0, and the one with $n = 1$ is Zone 1.

Due to the differences in the production process and application scenarios, there are zero-order, multiorder, and achromatic quarter-wave plates. The achromatic quarter-wave plates possess a flat spectral response to the broad-spectrum light source, but they are not commonly used in weak measurement because of the expense. Nevertheless, the period of

phase delay between the fast and slow axes of the multiorder quarter-wave plates cannot be accurately controllable, which is not suitable for the frequency domain weak measurements that require precise control of the time delay. Therefore, the effect of zero-order plates with spectrally dependent retardance is worthy of being further explored. In the SWV scheme applied in most cases, the standard preselection of elliptic polarization states is calculated only based on the central wavelength, which means that the analysis of phase retardation through QWP needs to be reconsidered for broad-spectrum light sources. Here we explore the effects of a standard zero-order waveplate with its spectrally dependent response. In the following, the concept of MWV is proposed to avoid the SWV scheme's deficiency.

III. MULTIPLE WEAK-VALUE MEASUREMENT

The weak measurement model based on the SWV in Zone 1 has become a powerful tool for the precision measurement of time delay. According to the theory above, the intensity of wavelength shift is proportional to the quadratic of the spectral width. This section investigates Zone 0 with higher sensitivity by analyzing the broad-spectrum source couple to the weak measurement system. In the weak measurement theory based on the frequency domain, the measurement accuracy is positively correlated with the bandwidth of the light source [39]. In this section, the zero-order quarter-wave plate is taken into account to deal with its spectrally dependent response for broad-spectrum light sources. For the ray with the design wavelength of QWP, the phase difference between ordinary ray and extraordinary ray through the wave plate is given by

$$\Gamma_0 = \frac{2\pi}{\lambda_0} (n_s - n_f) d = \frac{\pi}{2}. \quad (15)$$

Since the amount of delay corresponding to the broad-spectrum light is constant, the optical path difference generated by the QWP can be obtained;

$$(n_s - n_f) d = \frac{\lambda_0}{4}. \quad (16)$$

It is not hard to obtain $\Gamma \propto 1/\lambda$, the phase delay relationship in Eq. (15), after considering the adjacent wavelength of finite spectrum source can be rewritten as

$$\Gamma_m = \frac{2\pi}{\lambda} (n_s - n_f) d = \frac{2\pi}{\lambda} \frac{\lambda_0}{4} = \frac{\pi\lambda_0}{2\lambda}. \quad (17)$$

We define Γ_m as the modified phase delay, representing the conversion relationship of QWP at each wavelength. For broad-spectrum light sources, the Γ_m varies with each wavelength which is shown in Fig. 2(a). Therefore, the Jones matrix of the wavelength-dependent modified phase delay of QWP set to $\pi/4$ could be obtained:

$$\begin{aligned} &\begin{bmatrix} \cos \frac{\pi}{4} & -\sin \frac{\pi}{4} \\ \sin \frac{\pi}{4} & \cos \frac{\pi}{4} \end{bmatrix} \begin{bmatrix} e^{-i\frac{\Gamma_m}{2}} & 0 \\ 0 & e^{-i\frac{\Gamma_m}{2}} \end{bmatrix} \begin{bmatrix} \cos \frac{\pi}{4} & \sin \frac{\pi}{4} \\ -\sin \frac{\pi}{4} & \cos \frac{\pi}{4} \end{bmatrix} \\ &= \begin{bmatrix} \cos \frac{\Gamma_m}{2} & -i \sin \frac{\Gamma_m}{2} \\ -i \sin \frac{\Gamma_m}{2} & \cos \frac{\Gamma_m}{2} \end{bmatrix} = \begin{bmatrix} \cos \frac{\pi\lambda_0}{4\lambda} & -i \sin \frac{\pi\lambda_0}{4\lambda} \\ -i \sin \frac{\pi\lambda_0}{4\lambda} & \cos \frac{\pi\lambda_0}{4\lambda} \end{bmatrix}. \end{aligned} \quad (18)$$

Combined with the Jones matrix for P1 with the angle being set to $\pi/4 + \varepsilon$ in the previous section, the modified

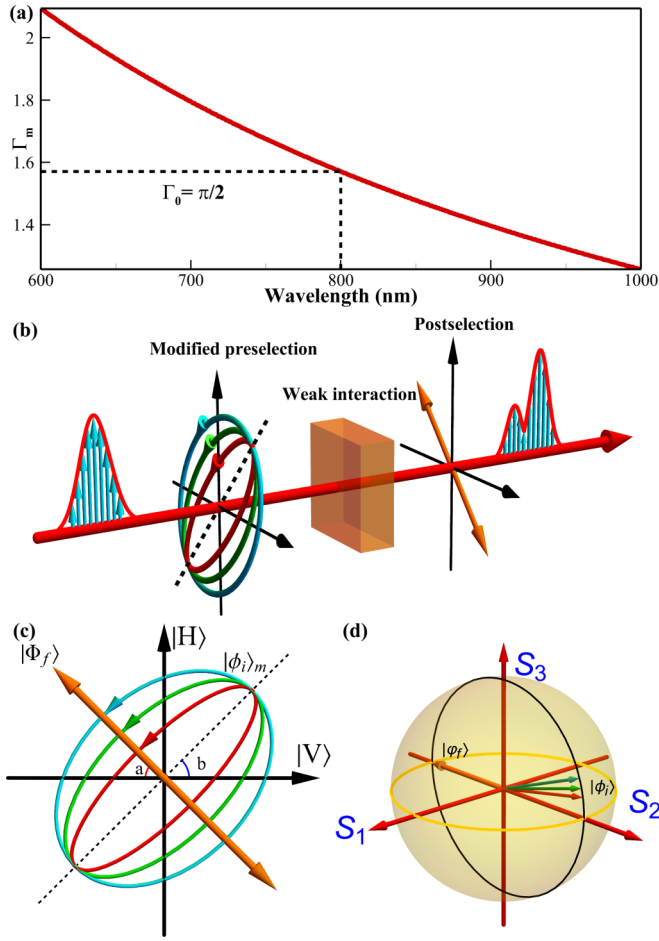


FIG. 2. Graphical presentation of the MWV scheme. (a) Schematic illustration of the MWV scheme based on the modified preselection. (b) Diagram of the modified preselection with multiple elliptical polarization components and postselection with linear polarization, where the magnitudes of angles a and b are $\pi/4$. (c) Presentation of modified preselection and postselection states via the Poincaré sphere. (d) The modified phase difference of the QWP (Γ_m) varies with different wavelengths in the broad-spectrum source, and the dashed line here indicates the phase difference of the central wavelength of the broad-spectrum source Γ_0 .

preselected state can be written as

$$\begin{aligned} & \begin{bmatrix} \cos \frac{\pi\lambda_0}{4\lambda} & -i \sin \frac{\pi\lambda_0}{4\lambda} \\ -i \sin \frac{\pi\lambda_0}{4\lambda} & \cos \frac{\pi\lambda_0}{4\lambda} \end{bmatrix} \begin{bmatrix} \cos^2(\frac{\pi}{4} + \varepsilon) & \frac{1}{2} \cos 2\varepsilon \\ \frac{1}{2} \cos 2\varepsilon & \sin^2(\frac{\pi}{4} + \varepsilon) \end{bmatrix} \begin{bmatrix} 1 \\ 1 \end{bmatrix} \\ & = \begin{bmatrix} e^{-i\frac{\pi\lambda_0}{4\lambda}} (\cos \varepsilon - e^{i\frac{\pi\lambda_0}{2\lambda}} \sin \varepsilon) \\ e^{-i\frac{\pi\lambda_0}{4\lambda}} (\cos \varepsilon + e^{i\frac{\pi\lambda_0}{2\lambda}} \sin \varepsilon) \end{bmatrix}. \end{aligned} \quad (19)$$

As a result, the modified preselection of the MWV scheme is obtained as

$$\begin{aligned} |\phi_i\rangle_m & = \frac{1}{\sqrt{2}} \left[e^{-i\frac{\pi\lambda_0}{4\lambda}} (\cos \varepsilon - e^{i\frac{\pi\lambda_0}{2\lambda}} \sin \varepsilon) |H\rangle \right. \\ & \quad \left. + e^{-i\frac{\pi\lambda_0}{4\lambda}} (\cos \varepsilon + e^{i\frac{\pi\lambda_0}{2\lambda}} \sin \varepsilon) |V\rangle \right]. \end{aligned} \quad (20)$$

Since the wavelength affects the elliptical polarization ellipticity in the modified preselection, the modified preselection

state of the broad-spectrum light source should be in the form of a combination of elliptical polarization states with different ellipticity. The schematic illustration of the MWV scheme is shown in Fig. 2(b), where the wave-function distribution in this case after passing through the system exhibits an incomplete separation of Gaussian form. Different from the general situation, Eq. (20) represents modified preselection in the weak measurement system, which is graphically shown in Fig. 2(c). For more clearly comparing, the modified preselection and the postselection states on a Poincaré sphere are shown in Fig. 2(d).

Due to the existence of the modified preselection, the weak value here is no longer the same as the purely imaginary one in the SWV scheme. And combining with $\omega = 2\pi c/\lambda$, the MWV contains both real and imaginary parts, which is obtained as

$$\begin{aligned} A_{\omega m} & = \frac{\langle \varphi_f | \hat{A} | \phi_i \rangle_m}{\langle \varphi_f | \phi_i \rangle_m} = \text{Re}(A_{\omega m}) + i \text{Im}(A_{\omega m}) \\ & = -\cos\left(\frac{\pi\omega}{2\omega_0}\right) \cot \varepsilon + i \sin\left(\frac{\pi\omega}{2\omega_0}\right) \cot \varepsilon. \end{aligned} \quad (21)$$

After selecting a preselected angle ε , the relation between the weak value and wavelength is shown in Fig. 3. The MWV in the modified weak measurement can be divided into real and imaginary parts, which correspond to the conditional mean value of observable under the restriction of zero interference and the system fluctuation in the weak measurement, respectively [17,42]. As shown in Fig. 3, the trend of the imaginary part is nearly not affected by the spectrum characteristics of the light source. However, the real part of the weak value can change rapidly in a small range of the preselection angle or the wavelength. The MWV in the modified theory is formed by accumulating the weak values corresponding to different wavelengths of the broad-spectrum Gaussian source.

Considering the modified preselection, the whole state with the Gaussian spectral distribution selected by $|\phi_i\rangle_m$ is written as

$$\begin{aligned} |\psi_m\rangle & = \int d\omega \frac{f(\omega)}{\sqrt{2}} \left[e^{-i\frac{\pi\omega}{4\omega_0}} (\cos \varepsilon - e^{i\frac{\pi\omega}{2\omega_0}} \sin \varepsilon) |H\rangle \right. \\ & \quad \left. + e^{-i\frac{\pi\omega}{4\omega_0}} (\cos \varepsilon + e^{i\frac{\pi\omega}{2\omega_0}} \sin \varepsilon) |V\rangle \right] |\omega\rangle. \end{aligned} \quad (22)$$

After the weak interaction between $|H\rangle$ and $|V\rangle$, the time delay is introduced and it becomes

$$\begin{aligned} |\psi'_m\rangle & = \int d\omega \frac{f(\omega)}{\sqrt{2}} \left[e^{-i\omega(\frac{\pi}{4\omega_0} - \tau)} (\cos \varepsilon - e^{i\frac{\pi\omega}{2\omega_0}} \sin \varepsilon) |H\rangle \right. \\ & \quad \left. + e^{-i\omega(\frac{\pi}{4\omega_0} + \tau)} (\cos \varepsilon + e^{i\frac{\pi\omega}{2\omega_0}} \sin \varepsilon) |V\rangle \right] |\omega\rangle. \end{aligned} \quad (23)$$

When the light passes through the postselection element, the wave function is converted into

$$\begin{aligned} \langle \varphi_f | \psi'_m \rangle & = \int d\omega \frac{f(\omega)}{2} \left[e^{-i\omega(\frac{\pi}{4\omega_0} - \tau)} (\cos \varepsilon - e^{i\frac{\pi\omega}{2\omega_0}} \sin \varepsilon) \right. \\ & \quad \left. - e^{-i\omega(\frac{\pi}{4\omega_0} + \tau)} (\cos \varepsilon + e^{i\frac{\pi\omega}{2\omega_0}} \sin \varepsilon) \right] |\omega\rangle. \end{aligned} \quad (24)$$

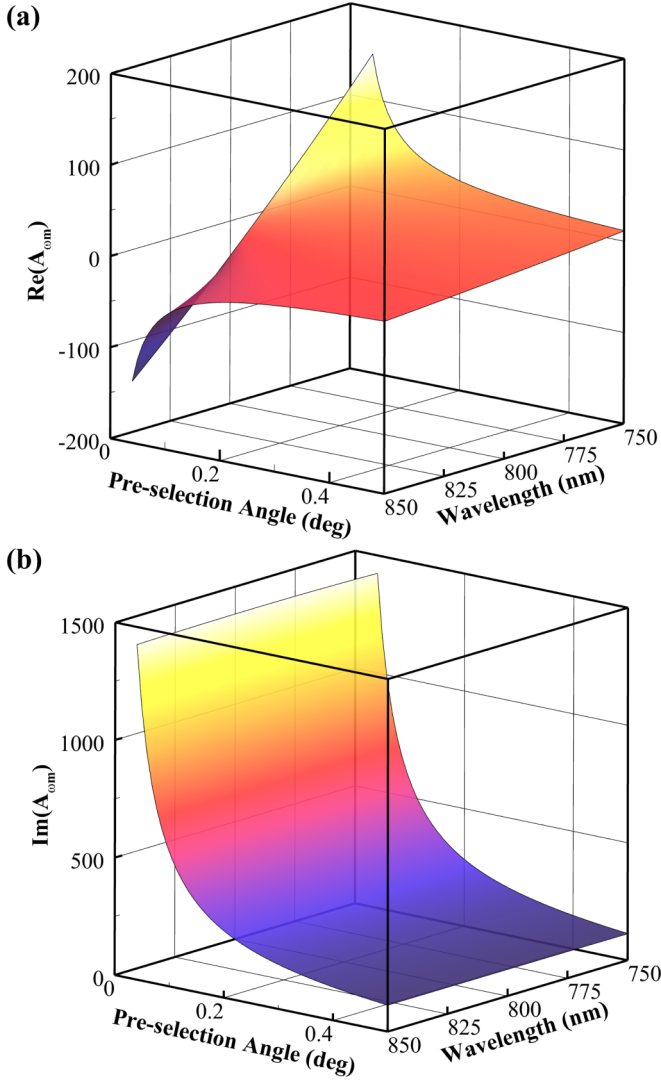


FIG. 3. (a) $\text{Re}(A_{om})$ and (b) $\text{Im}(A_{om})$ of the MWV scheme as a function of preselection angle and wavelength.

The corresponding postselection probability of modified weak measurements is

$$T_m = \frac{1}{4A} \left[2A - 2B \cos 2\varepsilon \cos(2\tau\omega_0) - \left(1 + e^{\frac{\pi\sigma^2\tau}{\omega_0}} \right) \sin 2\varepsilon \sin(2\tau\omega_0) \right], \quad (25)$$

where $A = \exp[\sigma^2(\pi + 4\tau\omega_0)^2/16\omega_0^2]$ and $B = \exp[\pi\sigma^2(\pi + 8\tau\omega_0)/16\omega_0^2]$.

In Fig. 4, the postselection probability of the weak measurement for SWV and MWV schemes varying with the time delay is illustrated. In terms of the range from 0 to 15 000 *as* in Fig. 4(a), it is impossible to distinguish the difference between the two models. However, there is virtually a difference in a narrower range in Fig. 4(b). In particular, the insets with the orange box and the green box show a closeup of the two working ranges of Zone 0 and Zone 1, respectively. The discrepancy in postselection probability between the two

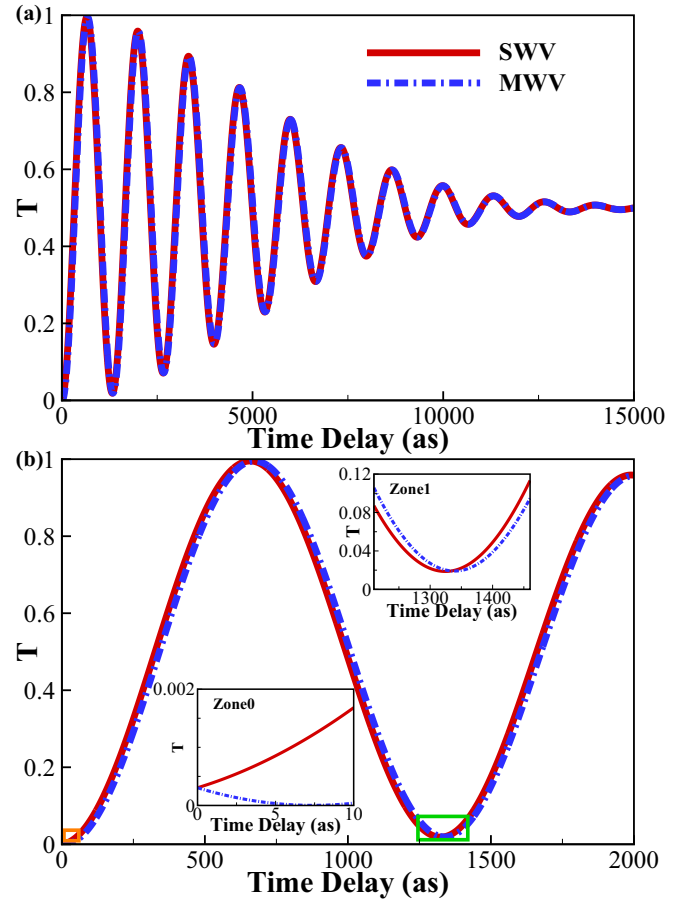


FIG. 4. (a) Postselection probability of the SWV scheme and the MWV scheme. (b) The probability from 0 to 2000 *as* to show the distinction between these two schemes. The orange and green boxes identify the working ranges of Zone 0 and Zone 1, respectively. The spectrum width is chosen as 50 nm and ε is set to 1 degree.

schemes in Zone 0 significantly impacts on subsequent amplification performance.

Finally, based on the wave-function state and the postselection probability, the frequency shift of the MWV scheme can be obtained as

$$\Delta\omega_m = \frac{\sigma^2 \cos(2\tau\omega_0)}{16A\omega_0 T_m} \left\{ \left[e^{\frac{\pi\sigma^2\tau}{\omega_0}} (\pi - 4\tau\omega_0) - 4\tau\omega_0 - \pi \right] \sin 2\varepsilon + 8B\tau\omega_0 \tan(2\tau\omega_0) \cos 2\varepsilon \right\}. \quad (26)$$

Similarly, the corresponding wavelength shift can be calculated from the frequency shift, yielding

$$\Delta\lambda_m = \frac{\lambda_0 \sigma^2 \cos(2\tau\omega_0)}{32\pi c A \omega_0 T_m} \left\{ \left[e^{\frac{\pi\sigma^2\tau}{\omega_0}} (4\tau\omega_0 - \pi) + 4\tau\omega_0 + \pi \right] \sin 2\varepsilon - 8B\omega_0 \tau \tan(2\tau\omega_0) \cos 2\varepsilon \right\}. \quad (27)$$

The linear-amplification region for sensitive measurement of time delay has been confirmed in previous work [8,43]. To show the differences in SWV and MWV schemes, we explore them in detail. The central wavelength is chosen as 800 nm, and the preselection angle is set to 1° for simulation.

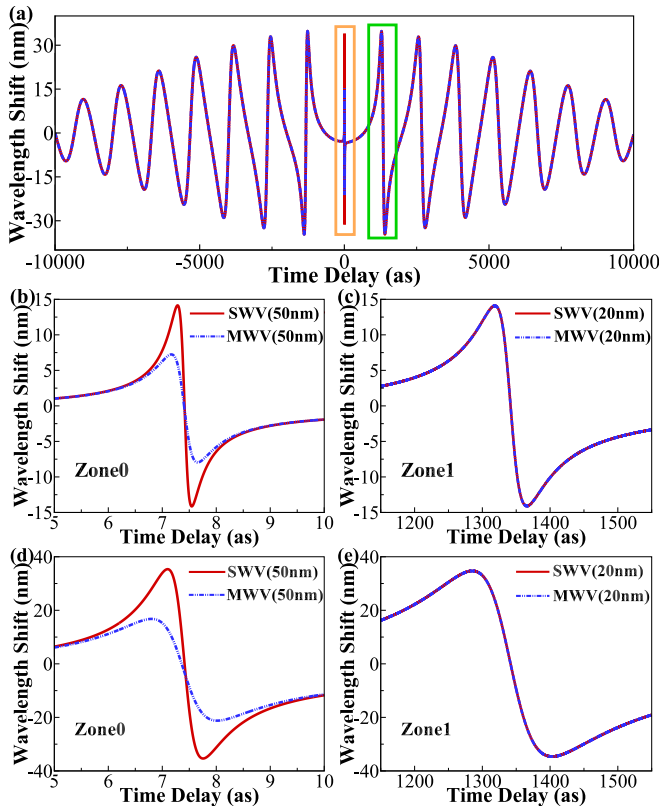


FIG. 5. (a) Wavelength shift $\Delta\lambda$ for the MWV scheme and SWV scheme as a function of time delay τ with the situation of 50-nm spectrum width and 1° preselection angle. The orange and green boxes highlight Zone 0 and Zone 1, respectively. (b) and (c) The wavelength shifts in Zone 0 and Zone 1 are shown with 20-nm spectral width of light source. (d) and (e) The comparison is given with the spectral width of light source being set to 50 nm.

In Fig. 5(a), the periodic evolution of the wavelength shift changing with time delay is presented based on Eqs. (14) and (27), and the spectral width of the light source is set to 50 nm. The orange box marks the region of Zone 0 with the highest measurement resolution, and the following Zone 1 in the green box has the second-highest resolution. In order to demonstrate the necessity of WVM schemes with varied measurement accuracy, two groups' bandwidths of 20-nm bandwidth and 50-nm bandwidth are presented here for comparative analysis. The first group constituted by Figs. 5(b) and 5(c) is the presentation of the two working regions with a spectral width of 20 nm, while Figs. 5(d) and 5(e) are the second group with a spectral width of 50 nm. In Fig. 5(b), the comparison between the SWV the MWV schemes in Zone 0 is exhibited. It was found that the wavelength shift amplitude of the MWV scheme is smaller than that of the SWV scheme, which means that the SWV scheme overestimates the measurement accuracy in theory. And it is harsh to differentiate the two schemes in the Fig. 5(c), which means that both schemes are competent for the work within Zone 1.

To achieve higher measurement accuracy when the 50-nm spectral width of the light source is applied, the comparison of two schemes is presented in Fig. 5(d). And the wavelength shift of the MWV scheme reaches 10 nm with

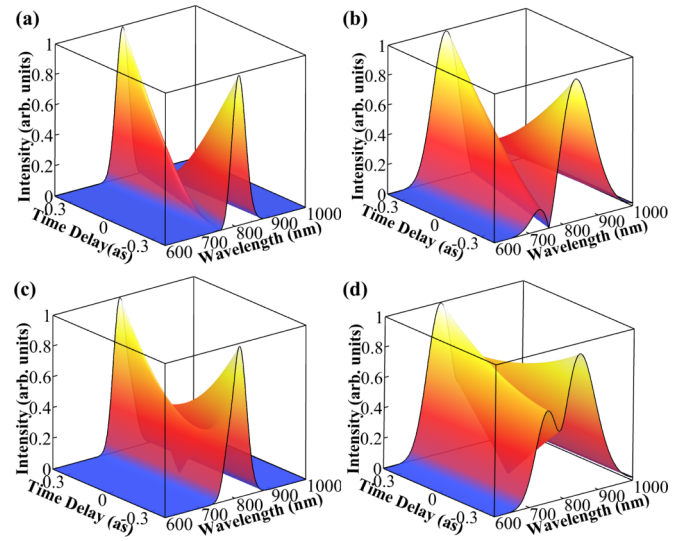


FIG. 6. Intensity of the SWV scheme in Zone 0 is shown with (a) 20-nm and (b) 50-nm spectral width of light source. For comparison, the intensity evolution for the MWV scheme with the widths (c) 20 nm and (d) 50 nm is plotted.

0.164as, whose rate of change can reach 60.98 nm/as. The two schemes' contrast in Zone 1 is illustrated in Fig. 5(e), which is also indistinguishable. The MWV scheme can obtain 10-nm wavelength shift at 8.6as with the rate of change reaching 1.16 nm/as in Zone 1. It can also be seen from Fig. 5 that the coincidence degree of MWV theory and SWV theory in the linear working region at 50 nm is significantly worse than that at 20 nm. This is ascribed to the different retardation for different wavelengths when light beam passes through the optical elements. But due to the lower sensitiveness in Zone 1, the spectral width of the light source does not affect the applicability of the SWV scheme for Zone 1.

In the frequency domain weak measurement, the wavelength shift is obtained from the centroid of the final spectral distribution, which is characterized by the change of the Gaussian splitting waveform. By comparing the intensity of the two schemes in Fig. 6, the wavelength shift affected by the time delay and wavelength can be obtained. As Figs. 6(a) and 6(b) shown, the variation of intensity with 20-nm and 50-nm spectral widths are compared in the SWV scheme. The Gaussian splitting waveform in the MWV scheme is distinguished from the complete splitting one in the SWV scheme, which is shown in Figs. 6(c) and 6(d). Two splitting components still overlap in Zone 0 due to the broadband spectral properties. It can also be inferred from a smaller wavelength shift of the MWV scheme compared with the one of the SWV scheme in Fig. 6.

In addition to accurately measuring time delay, this weak measurement scheme can also measure tiny polarization rotation. Similarly, the broadband spectral property also affects the angle measurement based on the emergence of modified preselection states. The wavelength shift of the SWV and MWV schemes as a function of the preselection angle has been shown in Fig. 7. The difference between the two schemes is also related to the spectral width. The amplitude of the wavelength shift in the MWV scheme is smaller than

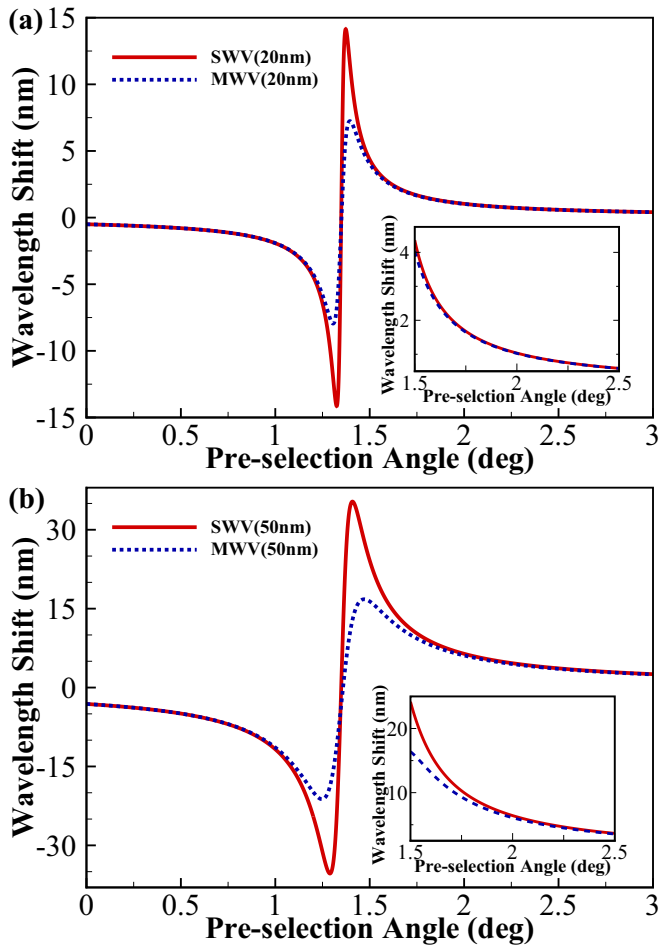


FIG. 7. Wavelength shift of the two schemes varies with the preselection angle. (a) and (b) The comparison between the single weak-value model and the multiple weak-value model with a spectral width of 20 nm and 50 nm, respectively. The insets show the situation of the preselection angle from 1.5° to 2.5° .

the one in the SWV scheme for a fixed preselection angle, which means that the prediction of the angle measurement in the SWV scheme for Zone 0 may be a deviation. For more obvious comparison, the insets show the difference between the two schemes in a smaller range from 1.5° to 3° . The SWV scheme becomes inaccurate for the measurement with wider spectral width 50 nm in this nonlinear region.

The time delay caused by weak interaction is a direct tiny effect in the frequency domain weak measurements. With a periodic change in the resulting wavelength shift, there is a working region with linear relation between wavelength shift and time delay. The Zone 1 mentioned above can abundantly demonstrate the measurement accuracy in recent works. Although the SWV scheme shows a higher accuracy, the MWV scheme can more precisely measure time delay based on a more accurate theoretical model. Therefore, the difference between the two models can improve the measurement accuracy by decreasing the time delay to achieve the sharper working region, namely Zone 0. Considering the detection resolution of a receiving instrument is 0.01 nm, the measurement

resolution of Zone 0 and Zone 1 based on the MWV is 1.6×10^{-4} as and 8.6×10^{-3} as, respectively. This indicates that the MWV scheme in Zone 0 can almost improve two orders of magnitude of the accuracy compared with the resolution based on Zone 1. However, higher precision measurement also means a higher sensitivity in the experimental manipulation that may be limited by technical issues, such as the light source stability, unwanted movement caused by rotating optical elements, and the resolution of detection equipment.

For weak measurements, various improvements with a diversity of theory have been proposed for more accurate detection [18,31,44–47]. The improved weak measurement with multiple weak values proposed here aims to predict the sensitive zones more accurately. In Zone 1 with lower measurement resolution, both SWV and MWV schemes are applicable for using the zero-order QWP in weak measurement experiments. However, the SWV scheme becomes inaccurate for Zone 0 with extremely high resolution. Therefore, the MWV scheme proposed in this work is significant for the experimental setup with the zero-order QWP. Although the current experimental conditions are not adequate for measurement in Zone 0, we believe the MWV scheme provided in this work can significantly improve the existing measurement experiment.

IV. CONCLUSIONS

In this paper, a weak measurement scheme with MWV is proposed to handle the influence of a broad-spectrum light source on modified preselection. The detailed deduction of the MWV amplification in the weak measurements is presented. The preselection is the superposition of elliptically polarized ellipses with different ellipticity for a linearly polarized incidence case. As a result, the complex MWVs and the deformation of spectral distribution appear, leading to postselection probability change. Comparing the standard SWV scheme with the MWV scheme, the significance and necessity of the modified scheme are verified in the two linear amplification regions, namely Zone 0 and Zone 1. For Zone 1, both the SWV and the MWV schemes are valid to detect the slight time delay based on broad-spectrum light source [7–9]. But for the region with a higher sensitivity (Zone 0), the SWV scheme and the MWV scheme have perceptible discrepancy and the MWV scheme can more precisely measure the time delay.

The dependence on other parameters can allow this WMV system for precision metrology. However, the prerequisite is a very accurate prediction of the measuring system, especially for the high-accuracy region of Zone 0. Since every weak measurement in the frequency domain operates with broad-spectrum light sources [34–38], the multiple-state effect is always present in the birefringence elements and inevitably affect the spectral distribution. Therefore, the MWV effect must be taken into account for future investigation of optical devices in spectral weak measurements.

ACKNOWLEDGMENTS

This work was supported by the National Natural Science Foundation of China (Grant No. 61835004) and Natural Science Foundation of Hunan Province (Grant No. 2021JJ10008).

- [1] N. Ritchie, J. G. Story, and R. G. Hulet, Realization of a Measurement of a “Weak Value”, *Phys. Rev. Lett.* **66**, 1107 (1991).
- [2] P. B. Dixon, D. J. Starling, A. N. Jordan, and J. C. Howell, Ultrasensitive Beam Deflection Measurement via Interferometric Weak Value Amplification, *Phys. Rev. Lett.* **102**, 173601 (2009).
- [3] P. Egan and J. A. Stone, Weak-value thermostat with 0.2 mk precision, *Opt. Lett.* **37**, 4991 (2012).
- [4] X. Zhou, X. Ling, H. Luo and S. Wen, Identifying graphene layers via spin Hall effect of light, *Appl. Phys. Lett.* **101**, 251602 (2012).
- [5] X. Qiu, X. Zhou, D. Hu, J. Du, F. Gao, Z. Zhang, and H. Luo, Determination of magneto-optical constant of Fe films with weak measurements, *Appl. Phys. Lett.* **105**, 131111 (2014).
- [6] J. Martínez-Rincón, C. A. Mullarkey, G. I. Viza, W.-T. Liu, and J. C. Howell, Ultrasensitive inverse weak-value tilt meter, *Opt. Lett.* **42**, 2479 (2017).
- [7] G. I. Viza, J. Martínez-Rincón, G. A. Howland, H. Frostig, I. Shomroni, B. Dayan, and J. C. Howell, Weak-values technique for velocity measurements, *Opt. Lett.* **38**, 2949 (2013).
- [8] L. J. Salazar-Serrano, D. Janner, N. Brunner, V. Pruneri, and J. P. Torres, Measurement of sub-pulse-width temporal delays via spectral interference induced by weak value amplification, *Phys. Rev. A* **89**, 012126 (2014).
- [9] H. Li, J.-Z. Huang, Y. Yu, Y. Li, C. Fang, and G. Zeng, High-precision temperature measurement based on weak measurement using nematic liquid crystals, *Appl. Phys. Lett.* **112**, 231901 (2018).
- [10] Y. Aharonov, D. Z. Albert, and L. Vaidman, How the Result of a Measurement of a Component of the Spin of a Spin-1/2 Particle Can Turn Out to be 100, *Phys. Rev. Lett.* **60**, 1351 (1988).
- [11] R. Jozsa, Complex weak values in quantum measurement, *Phys. Rev. A* **76**, 044103 (2007).
- [12] A. Peres, Quantum Measurements with Postselection, *Phys. Rev. Lett.* **62**, 2326 (1989).
- [13] I. Duck, P. M. Stevenson, and E. Sudarshan, The sense in which a “weak measurement” of a spin-1/2 particle’s spin component yields a value 100, *Phys. Rev. D* **40**, 2112 (1989).
- [14] S. Kocsis, B. Braverman, S. Ravets, M. J. Stevens, R. P. Mirin, L. K. Shalm, and A. M. Steinberg, Observing the average trajectories of single photons in a two-slit interferometer, *Science* **332**, 1170 (2011).
- [15] J. S. Lundeen, B. Sutherland, A. Patel, C. Stewart, and C. Bamber, Direct measurement of the quantum wavefunction, *Nature (London)* **474**, 188 (2011).
- [16] O. Hosten and P. Kwiat, Observation of the spin Hall effect of light via weak measurements, *Science* **319**, 787 (2008).
- [17] J. Dressel, Weak values as interference phenomena, *Phys. Rev. A* **91**, 032116 (2015).
- [18] D. J. Starling, P. B. Dixon, N. S. Williams, A. N. Jordan, and J. C. Howell, Continuous phase amplification with a Sagnac interferometer, *Phys. Rev. A* **82**, 011802(R) (2010).
- [19] M. Pfeifer and P. Fischer, Weak value amplified optical activity measurements, *Opt. Express* **19**, 16508 (2011).
- [20] X. Zhou, Z. Xiao, H. Luo, and S. Wen, Experimental observation of the spin Hall effect of light on a nanometal film via weak measurements, *Phys. Rev. A* **85**, 043809 (2012).
- [21] L. Zhou, Y. Turek, C. Sun, and F. Nori, Weak-value amplification of light deflection by a dark atomic ensemble, *Phys. Rev. A* **88**, 053815 (2013).
- [22] J. Liu, K. Zeng, W. Xu, S. Chen, H. Luo, and S. Wen, Ultrasensitive detection of ion concentration based on photonic spin Hall effect, *Appl. Phys. Lett.* **115**, 251102 (2019).
- [23] R. Wang, J. Zhou, K. Zeng, S. Chen, X. Ling, W. Shu, H. Luo, and S. Wen, Ultrasensitive and real-time detection of chemical reaction rate based on the photonic spin Hall effect, *APL Photonics* **5**, 016105 (2020).
- [24] S. Chen, X. Ling, W. Shu, H. Luo, and S. Wen, Precision Measurement of the Optical Conductivity of Atomically Thin Crystals via the Photonic Spin Hall Effect, *Phys. Rev. Applied* **13**, 014057 (2020).
- [25] S. Pang, J. Dressel, and T. A. Brun, Entanglement-Assisted Weak Value Amplification, *Phys. Rev. Lett.* **113**, 030401 (2014).
- [26] G. Chen, L. Zhang, W.-H. Zhang, X.-X. Peng, L. Xu, Z.-D. Liu, X.-Y. Xu, J.-S. Tang, Y.-N. Sun, and D.-Y. He, Achieving Heisenberg-scaling Precision with Projective Measurement on Single Photons, *Phys. Rev. Lett.* **121**, 060506 (2018).
- [27] G. Chen, N. Aharon, Y.-N. Sun, Z.-H. Zhang, W.-H. Zhang, D.-Y. He, J.-S. Tang, X.-Y. Xu, Y. Kedem, and C.-F. Li, Heisenberg-scaling measurement of the single-photon Kerr non-linearity using mixed states, *Nat. Commun.* **9**, 1 (2018).
- [28] S. Pang and T. A. Brun, Improving the Precision of Weak Measurements by Postselection Measurement, *Phys. Rev. Lett.* **115**, 120401 (2015).
- [29] A. G. Kofman, S. Ashhab, and F. Nori, Nonperturbative theory of weak pre-and post-selected measurements, *Phys. Rep.* **520**, 43 (2012).
- [30] Y. Susa, Y. Shikano, and A. Hosoya, Optimal probe wave function of weak-value amplification, *Phys. Rev. A* **85**, 052110 (2012).
- [31] J. Dressel, K. Lyons, A. N. Jordan, T. M. Graham, and P. G. Kwiat, Strengthening weak-value amplification with recycled photons, *Phys. Rev. A* **88**, 023821 (2013).
- [32] N. Brunner and C. Simon, Measuring Small Longitudinal Phase Shifts: Weak Measurements or Standard Interferometry? *Phys. Rev. Lett.* **105**, 010405 (2010).
- [33] B. de Lima Bernardo, S. Azevedo, and A. Rosas, Ultrasensitive polarization rotation measurements via weak value amplification, *Phys. Lett. A* **378**, 2029 (2014).
- [34] X.-Y. Xu, Y. Kedem, K. Sun, L. Vaidman, C.-F. Li, and G.-C. Guo, Phase Estimation with Weak Measurement Using a White Light Source, *Phys. Rev. Lett.* **111**, 033604 (2013).
- [35] Y. Zhang, D. Li, Y. He, Z. Shen, and Q. He, Optical weak measurement system with common path implementation for label-free biomolecule sensing, *Opt. Lett.* **41**, 5409 (2016).
- [36] D. Li, T. Guan, F. Liu, A. Yang, Y. He, Q. He, Z. Shen, and M. Xin, Optical rotation based chirality detection of enantiomers via weak measurement in frequency domain, *Appl. Phys. Lett.* **112**, 213701 (2018).
- [37] Y. Wang, S. Chen, S. Wen, and H. Luo, Realization of ultra-small stress birefringence detection with weak-value amplification technique, *Appl. Phys. Lett.* **118**, 161104 (2021).
- [38] Y. He, L. Luo, L. Xie, J. Shao, Y. Liu, J. You, Y. Ye, and Z. Zhang, Detection of Magneto-optical Kerr signals via weak measurement with frequency pointer, *Opt. Lett.* **46**, 4140 (2021).

- [39] C.-F. Li, X.-Y. Xu, J.-S. Tang, J.-S. Xu, and G.-C. Guo, Ultrasensitive phase estimation with white light, *Phys. Rev. A* **83**, 044102 (2011).
- [40] Y. Aharonov and L. Vaidman, Properties of a quantum system during the time interval between two measurements, *Phys. Rev. A* **41**, 11 (1990).
- [41] A. N. Jordan, J. Martínez-Rincón, and J. C. Howell, Technical Advantages for Weak-Value Amplification: When Less is More, *Phys. Rev. X* **4**, 011031 (2014).
- [42] J. Dressel and A. N. Jordan, Significance of the imaginary part of the weak value, *Phys. Rev. A* **85**, 012107 (2012).
- [43] N. S. Williams and A. N. Jordan, Weak Values and the Leggett-Garg Inequality in Solid-State Qubits, *Phys. Rev. Lett.* **100**, 026804 (2008).
- [44] G. Strübi and C. Bruder, Measuring Ultrasmall Time Delays of Light by Joint Weak Measurements, *Phys. Rev. Lett.* **110**, 083605 (2013).
- [45] K. Lyons, J. Dressel, A. N. Jordan, J. C. Howell, and P. G. Kwiat, Power-Recycled Weak-Value-Based Metrology, *Phys. Rev. Lett.* **114**, 170801 (2015).
- [46] S. Chen, X. Zhou, C. Mi, H. Luo, and S. Wen, Modified weak measurements for the detection of the photonic spin Hall effect, *Phys. Rev. A* **91**, 062105 (2015).
- [47] Z.-H. Zhang, G. Chen, X.-Y. Xu, J.-S. Tang, W.-H. Zhang, Y.-J. Han, C.-F. Li, and G.-C. Guo, Ultrasensitive biased weak measurement for longitudinal phase estimation, *Phys. Rev. A* **94**, 053843 (2016).